The disordered P granule protein LAF-1 drives phase separation into droplets with tunable viscosity and dynamics

Shana Elbaum-Garfinkle[a], Younghoon Kim[b], Krzysztof Szczepaniak[c,d,e], Carlos Chih-Hsiung Chen[a], Christian R. Eckmann[c,d], Sua Myong[b], and Clifford P. Brangwynne[a,1]

[a]Department of Chemical and Biological Engineering, Princeton University, Princeton, NJ 08540; [b]Department of Bioengineering, University of Illinois at Urbana Champaign, Urbana, IL 61801; [c]Max Planck Institute of Molecular Cell Biology and Genetics, 01307 Dresden, Germany; [d]Department of Genetics, Martin-Luther-University, Halle-Wittenberg, 06108 Halle, Germany; and [e]Dresden International PhD Program, 01307 Dresden, Germany

P granules and other RNA/protein bodies are membrane-less organelles that may assemble by intracellular phase separation, similar to the condensation of water vapor into droplets. However, the molecular driving forces and the nature of the condensed phases remain poorly understood. Here, we show that the *Caenorhabditis elegans* protein LAF-1, a DDX3 RNA helicase found in P granules, phase separates into P granule-like droplets in vitro. We adapt a microrheology technique to precisely measure the viscoelasticity of micrometer-sized LAF-1 droplets, revealing purely viscous properties highly tunable by salt and RNA concentration. RNA decreases viscosity and increases molecular dynamics within the droplet. Single molecule FRET assays suggest that this RNA fluidization results from highly dynamic RNA–protein interactions that emerge close to the droplet phase boundary. We demonstrate than an N-terminal, arginine/glycine rich, intrinsically disordered protein (IDP) domain of LAF-1 is necessary and sufficient for both phase separation and RNA–protein interactions. In vivo, RNAi knockdown of LAF-1 results in the dissolution of P granules in the early embryo, with an apparent submicromolar phase boundary comparable to that measured in vitro. Together, these findings demonstrate that LAF-1 is important for promoting P granule assembly and provide insight into the mechanism by which IDP-driven molecular interactions give rise to liquid phase organelles with tunable properties.

liquid droplets | intracellular phase transition | intrinsically disordered proteins | RNA granules

Intracellular RNA/protein (RNP) assemblies, including germ granules, processing bodies, stress granules, and nucleoli, are key players in the regulation of gene expression (1). RNP bodies, also referred to as RNA granules, function in diverse modes of RNA processing, including splicing, degradation, and translational repression of mRNA. These ubiquitous structures lack a membrane boundary but nonetheless represent a coherent organelle composed of thousands of molecules, manifesting as microscopically visible puncta in both the cytoplasm and the nucleus.

Recent studies have demonstrated the apparent liquid-like behavior of various RNP bodies (2–5) including wetting, dripping, and relaxation to spherical structures upon fusion or shearing. The assembly and disassembly of liquid-like organelles appears to be governed by a phase separation process, demonstrated by a concentration-dependent condensation/dissolution of P granules (2, 6) and the assembly and size scaling of the nucleolus (7) in the *Caenorhabditis elegans* embryo. Liquid phase separation has also been suggested to play a role in stress granule assembly (4) and in multivalent signaling proteins (8). These studies lend increasing support to the hypothesis that liquid phases play a central role in intracellular organization. However, the specific molecular interactions that drive phase separation and the mechanisms by which liquid properties impart cellular function remain largely unclear.

P granules are implicated in germ cell lineage maintenance in *C. elegans* and may serve similar functions as polar granules or nuage, which regulate germ cell biology across animal cells (9). In the newly fertilized *C. elegans* embryo, P granules segregate to the embryo posterior, which upon cytokinesis, defines the first germ-line precursor cell. This P granule segregation process is controlled by the preferential dissolution of anterior P granules and their stabilization and condensation in the posterior. The spatial control of P granule phase behavior arises from the anterior–posterior axis of the embryo spanning a liquid–liquid demixing phase boundary (2, 10).

Despite our understanding of the overall features of P granule segregation, the molecular interactions controlling P granule assembly and their liquid-like biophysical properties remain poorly understood. Like other RNP bodies, P granules are enriched in RNA-binding proteins, including PGL-1,-3 and the RNA helicases CGH-1, GLH-1–4, LAF-1, and VBH-1 (11). Members of the highly conserved DDX3 subfamily of DEAD-box RNA helicases, including human DDX3X, yeast Ded1p, and *Drosophila* Belle, have demonstrated roles in the assembly and remodeling of RNPs (12–14). Interestingly, many of these RNA helicases are predicted to be partially disordered, consistent with bioinformatic analysis, suggesting disordered motifs are common in RNP bodies (15).

Significance

Phase transitions have recently emerged as a key mechanism for intracellular organization. However, the underlying molecular interactions and nature of the resulting condensed phases are poorly understood. Here, we identify a role for LAF-1 in the liquid phase separation of P granules—RNA/protein assemblies implicated in germ-line maintenance. We adapt microrheology techniques to measure precise viscoelastic properties of LAF-1 liquid droplets. Our experiments reveal that electrostatic disordered protein interactions give rise to droplets with tunable material properties. RNA can fluidize protein droplets by decreasing the viscosity and increasing internal molecular dynamics. Our results provide insight into the mechanism by which molecular level interactions can give rise to liquid phase organelles with tunable material properties, potentially underlying biologically adaptable functions.
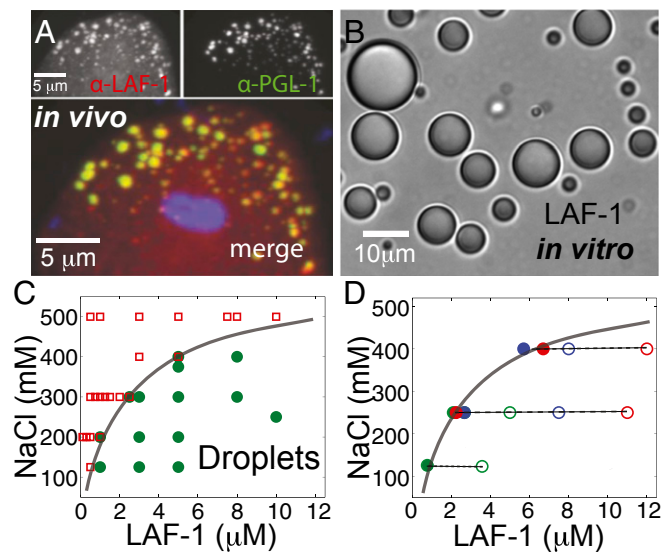
BIOPHYSICS AND COMPUTATIONAL BIOLOGY

Fig. 1. LAF-1 colocalizes to P granules in vivo and phase separates into droplets in vitro. (*A*) Confocal images of two-cell embryo posterior immunostained for LAF-1 (*Upper Left*) and PGL-1 (*Upper Right*). In the dividing P1 cell, LAF-1 localizes to PGL-1–marked P granules; DAPI-stained nucleus is included in the merged image. (*B*) DIC image of phase separated LAF-1 droplets. (*C*) Protein/NaCl concentrations scoring positive (green circles) or negative (red squares) for optically resolvable droplets are plotted, resulting in a phase boundary (line drawn to guide the eye). (*D*) The protein concentration in the dilute phase (●) is plotted for varying total protein concentrations (○) at three different salt concentrations. For all conditions, the concentration of the dilute phase falls directly onto the LAF-1 phase boundary from *C* (solid line).

Intrinsically disordered protein (IDP) motifs typically have a strong bias in their amino acid sequences. These proteins and other proteins that are highly enriched in a small number of amino acids are referred to as low complexity sequences (LCSs). LCSs in proteins, such as that in the protein FUS, have emerged as potentially important motifs in driving phase transitions underlying RNP body assembly (16–18). However, LCS domains have been reported to undergo phase transitions into solid gels, which contrasts with the liquid-like behavior of intracellular RNP bodies. Because solid-like gel phases are expected to slow or inhibit molecular dynamics, while liquid-like droplet phases should

facilitate molecular dynamics, these studies raise important questions about the viscoelastic properties of LCS/IDP phases. However, measuring these rheological properties represents a formidable challenge, due to the small size and transient nature of RNP bodies. Elucidating the precise nature of these material properties is nonetheless an essential step toward understanding their impact on biological function (19).

Here we show that the DDX3 family RNA helicase LAF-1 plays a key role in promoting *C. elegans* P granule formation by driving liquid–liquid phase separation. We find that LAF-1 can phase separate in vitro into liquid droplets resembling P granules, as well as impact P granule assembly in the early embryo. To measure the material properties of these micrometer-sized droplets, we adapt a microrheology technique that uses Brownian motion of probe particles to extract their viscoelastic properties. Together with fluorescence recovery after photobleaching (FRAP) and single molecule experiments, our experiments reveal a role for the disordered arginine/glycine-rich (RGG) domain of LAF-1 in driving phase separation and promoting dynamic protein–RNA interactions. We show that electrostatic interactions give rise to droplets with tunable physical properties and protein dynamics. We further demonstrate that RNA can modulate droplet viscosity and dynamics, suggesting that the viscosity of P granules and other RNP bodies may be modulated to achieve diverse biological functions.

Results

LAF-1 Phase Separates into Condensed Liquid Droplets in Vitro. Previous work has shown that the *C. elegans* protein LAF-1 is essential for germ-line development, with a potential role in regulating sex determination (20). To quantify LAF-1 localization within *C. elegans* embryos, we developed an antibody that specifically recognizes LAF-1 (Fig. S1). Consistent with a previous report using a GFP-tagged LAF-1 construct (21), we find that endogenous LAF-1 exhibits a high degree of colocalization with PGL-1, the founding P granule protein (Fig. 1*A*).

To study LAF-1 using a bottom-up biochemical approach, we sought to purify recombinant LAF-1. During the course of these studies, we found that upon lowering the salt (NaCl) concentration of solutions of purified LAF-1, the solution became cloudy. On further inspection under the microscope, we find that this solution turbidity is the result of condensed, highly spherical droplets of LAF-1 (Fig. 1*B*). By direct microscopic imaging, we mapped the protein and salt concentrations at which LAF-1 condenses out of solution (Fig. 1*C*). To rule out the possibility that residual RNA may be bound to LAF-1 and responsible for
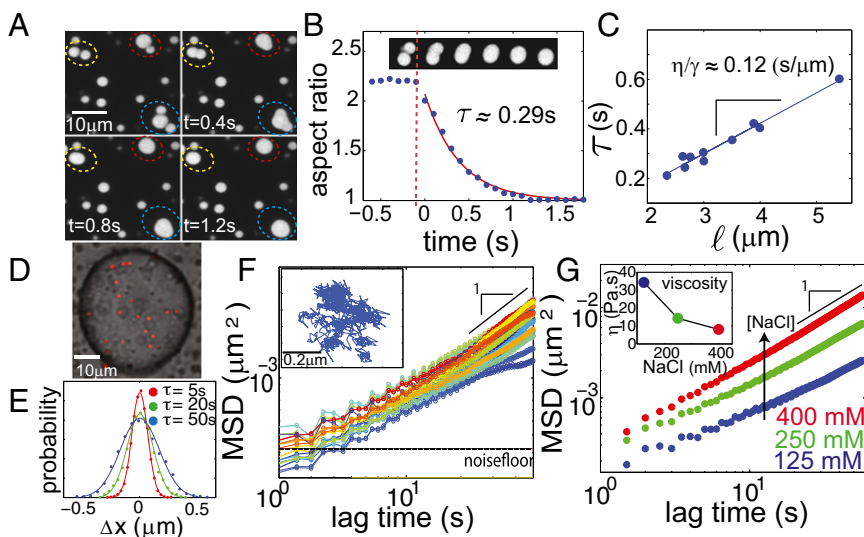

Fig. 2. LAF-1 droplets are homogeneous fluids with salt-dependent viscosity. (*A*) Confocal image sequence showing LAF-1 droplet fusion. (*B*) Fusion events are well fit by an exponential decay, which is used to determine fusion timescale τ. (*C*) Decay time vs. length scale for LAF-1 droplets prepared in 125 mM NaCl. The linear slope represents the inverse capillary velocity, $\eta/\gamma \approx 0.12$ s/μm. (*D*) Confocal image of red fluorescent beads embedded inside a large LAF-1 droplet. (*E*) Probability distribution of bead displacement for three different lag times. Distributions are well fit to a Gaussian (solid lines) indicating a homogenous environment. (*F*) Mean squared displacement vs. lag time. MSD data for individual beads from a single droplet are plotted. Black solid line, slope of 1; black dash, the noisefloor is $\approx 2 \times 10^{-4}$ μm. (*Inset*) Representative 2D particle track. (*G*) Increasing concentrations of NaCl result in increased MSD of particles and decreased viscosity (*Inset*).
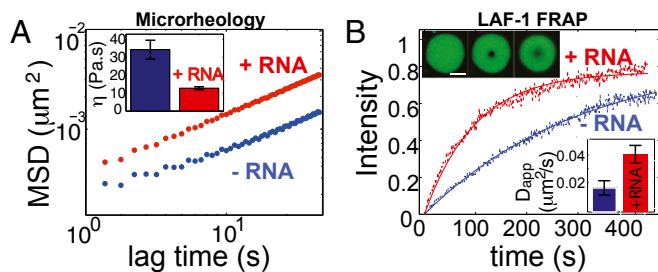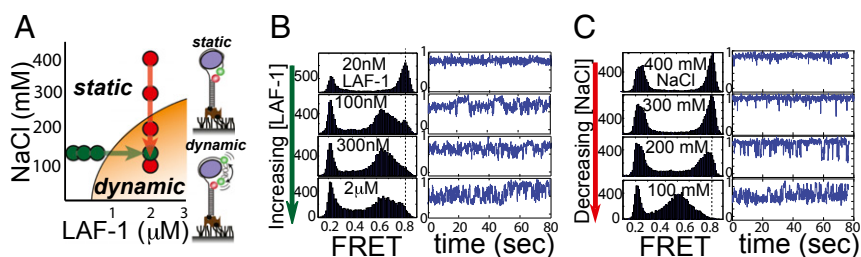
Fig. 3. RNA fluidizes LAF-1 droplets. (*A*) RNA addition (5 μM pU50) increases MSD of particles in LAF-1 droplets and decreases viscosity: (*Inset*) [NaCl] = 125 mM. (*B*) The timescale of LAF-1 FRAP recovery within droplets decreases on addition of 5 μM pU50 RNA (red). (*Upper Inset*) Representative droplets in which ≈ 1% of LAF-1 is labeled with DyLight 488: prebleach (*Left*), post-bleach (*Center*), and t ≈ 300 s (*Right*). (*Lower Inset*) Calculated apparent diffusion coefficients.

the observed salt-dependent phase behavior, we included a heparin affinity column in our protein purification (*SI Text*) to effectively compete for nucleotide binding. At 125 mM NaCl, LAF-1 begins condensing at a critical protein concentration of roughly 800 nM. Interestingly, this is the same order of magnitude as our estimated in vivo cytoplasmic concentration of LAF-1 (*SI Text*). Moreover, the in vitro LAF-1 droplets are reminiscent of the LAF-1–rich P granules observed in vivo (Fig. 1*A*), suggesting that LAF-1 may play a central role in driving P granule assembly.

At protein concentrations above a critical threshold, a system can separate into two phases: a dilute solution and condensed phase (22). Theory predicts that at equilibrium, the concentration in each phase will be fixed, and independent of total protein concentration, for a given set of conditions (23, 24). To test this prediction, we directly measured the concentration in the dilute phase upon removal of the droplets by centrifugation. For a given NaCl concentration, the concentration of soluble LAF-1 stays roughly constant, even for increasing total LAF-1 concentrations (Fig. 1*D*). Moreover, the concentration of the dilute phase lies directly on the phase boundary, determined from the point at which droplets are first observed (Fig. 1*C*). Thus, LAF-1 droplets are in equilibrium with a saturated protein solution outside of the droplets, consistent with a thermodynamically driven phase separation.

LAF-1 Droplets Are Homogenous Fluids with Tunable Viscosity. The biophysical properties of RNA/protein bodies are expected to affect their RNA regulatory function, because these properties (i.e., viscoelasticity and surface tension) will strongly impact molecular mobility and reactivity (3, 25). The highly spherical nature of in vitro LAF-1 droplets suggests they may represent simple viscous liquids, similar to previous reports describing the liquid-like nature of P granules (2, 6). Consistent with this, we frequently observe that when two or more LAF-1 droplets contact one another, they readily fuse and round up into a single larger sphere

(Fig. 2*A*). Analysis of these dynamics reveals that the shape of coalescing droplets (aspect ratio) exhibits an exponential relaxation to a sphere (Fig. 2*B*). For simple liquid droplets in a solution of lower viscosity, the characteristic fusion timescale would be given by $\tau \approx l(\eta/\gamma)$, where l is the average droplet radius, η is the viscosity of the droplet, γ is the surface tension, and the ratio η/γ is known as the inverse capillary velocity. Plotting τ vs. l for droplets at 125 mM NaCl shows a strong linear relationship, which yields $\eta/\gamma \approx 0.12$ s/μm (Fig. 2*C*); this is comparable to but somewhat faster than previous estimates of the inverse capillary velocity of native P granules (2, 6).

This fusion timescale analysis only allows us to estimate the ratio of viscosity to surface tension. To directly measure viscosity, we adapted a microrheology technique that was developed for probing the viscoelastic properties of small soft samples (5, 26). Polyethylene glycol (PEG)-passivated probe particles of radius $a = 0.5$ μm are incorporated into LAF-1 droplets, and their motion is tracked over time (Fig. 2*D*). We find that probe particles within the droplets exhibit random Brownian fluctuations, which are Gaussian distributed, consistent with a homogenous fluid at thermal equilibrium (Fig. 2*E*). For an equilibrium viscoelastic fluid, the mean-squared displacement (MSD) can grow as a power law in time: $\langle \Delta R^2 \rangle \sim t^\alpha$, where α is the diffusive exponent; for pure viscous fluids, $\alpha = 1$, whereas more complex viscoelastic properties give rise to so-called subdiffusive behavior, with $\alpha < 1$. We find that, away from the noise floor, the MSD of probe particles in LAF-1 droplets grows linearly with time ($\alpha = 1$), consistent with pure viscous properties on these timescales. Fitting the data to $\langle \Delta R^2 \rangle = 4Dt$ (Fig. S2), we obtain a diffusion coefficient, D, which can then be used to precisely determine the droplet viscosity, η, through the Stokes–Einstein relation: $D = k_B T/6\pi\eta a$, where $k_B T$ is the thermal energy scale. At physiological salt (125 mM NaCl), LAF-1 droplets have a viscosity of $\eta = 34 \pm 5$ Pa·s, which is similar to that of honey.

The strong dependence of the LAF-1 phase boundary on salt concentration (Fig. 1) suggests that electric charge plays an important role in the intermolecular LAF-1 interactions underlying droplet assembly. To test whether salt can also modulate the material properties of LAF-1 droplets, we assembled droplets at different salt concentrations and used microrheology to measure droplet viscosity. We find that with increasing salt concentration, the particle motion inside LAF-1 droplets increases, seen by a shift up in the MSD plot (Fig. 2*G*). The resulting droplet viscosity decreases to $\eta \approx 14$ and $\eta \approx 8$ Pa·s for 250 and 400 mM NaCl, respectively. Because the viscosity of a fluid reflects the effective strength of intermolecular interactions (27, 28), this viscosity decrease is consistent with the destabilizing effect of salt on droplet assembly (Fig. 1).

RNA Increases Fluidity and Dynamics Within LAF-1 Droplets. RNA is likely a major component of P granules in vivo and is a negatively charged polymer, which therefore might also influence LAF-1 droplet properties. Using a single-stranded poly-uridine model RNA (polyU 50), we find that LAF-1 binds RNA with high

Fig. 4. LAF-1–induced RNA dynamics activated near phase boundary. (*A*) LAF-1–RNA interactions are measured across the phase boundary by increasing the protein concentration (green arrow) and decreasing the NaCl concentration (red arrow). Measurements were performed at the indicated LAF-1 and NaCl concentrations (colored circles). (*B*) As the concentration of LAF-1 approaches the phase boundary, the peak at FRET values of ≈ 0.8 decreases, shifts, and broadens (*Left*). Single molecule FRET efficiency traces reveal dynamic pattern of LAF-1–RNA interactions emerging at increasing concentration (*Right*). [NaCl] held constant at 125 mM. (*C*) As the NaCl concentration approaches and crosses the phase boundary, the FRET peak similarly shifts and broadens (*Left*), concomitant with increased FRET dynamics (*Right*).
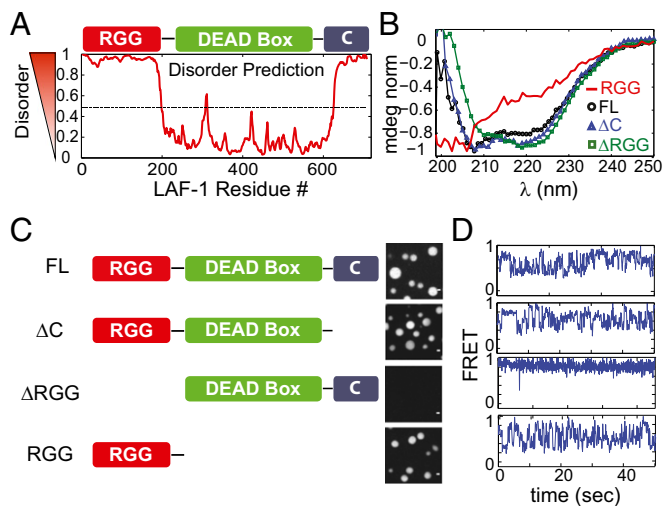
Fig. 5. Disordered N-terminal RGG domain drives phase separation and RNA/protein dynamics. (*A*) The PONDR algorithm predicts a high degree of disorder for both N and C termini of LAF-1. (*B*) Circular dichroism spectra indicate that the N-terminal RGG domain resembles a random coil, whereas FL, ∆C, and ∆RGG constructs contain secondary structure dominated by alpha helical conformation. (*C*) Schematic of LAF-1 deletion constructs. (*Right*) Droplets formed in 125 mM NaCl with DyLight-488–labeled protein for the indicated LAF-1 construct. (*D*) Single molecule FRET traces were recorded for 2 µM protein and 125 mM NaCl. The RGG domain is necessary and sufficient for dynamic RNA–protein interactions.

affinity ($K_D \approx 10$ nM), measured by a single molecule FRET binding assay ([Fig. S3](#)). Interestingly, although RNA partitions into the condensed phase, we do not observe a significant shift in the phase diagram upon RNA inclusion ([Fig. S4](#)). To test the impact of this charged high-affinity binding partner on droplet properties, we added polyU50 RNA to the phase-separating LAF-1 solution. We find that addition of 5 µM RNA into in vitro LAF-1 droplets (at 125 mM NaCl) results in a threefold decrease in the viscosity, with $\eta = 12.8 \pm 0.8$ Pa·s (Fig. 3*A*); this is consistent with rough estimates previously made to determine the apparent viscosity of in vivo P granules (2, 6). Together with the measured inverse capillary velocity, $\eta/\gamma \approx 0.12$ s/um, this yields a droplet surface tension of $\gamma \approx 100$ µN/m, consistent with low values typical of macromolecular liquids (29).

To determine whether RNA-induced fluidization of droplets is associated with increased protein diffusivity, we used FRAP to quantify molecular dynamics within LAF-1 droplets. We bleached a small spot ($R = 1.5$ µm) inside droplets containing ≤ 1% LAF-1 labeled with DyLight 488 (Fig. 3*B*). In the absence of RNA, LAF-1 recovers on a timescale of ~233 s, with an apparent diffusion coefficient of $D \approx 0.010$ µm^2/s. On addition of 5 µM unlabeled RNA, the recovery timescale of LAF-1 decreases more than twofold to ≈ 94 s, with an increase in the apparent diffusion coefficient to 0.024 µm^2/s (Fig. 3*B, Inset*). Repeating the experiment with low levels of fluorescently labeled RNA (250 nM), we find that mobility of RNA also increases, about ≈ 1.5-fold, upon addition of 5 µM unlabeled RNA ([Fig. S5](#)). Thus, the fluidization of LAF-1 droplets by RNA is accompanied by a corresponding increase in diffusive dynamics of both RNA and protein.

Dynamics of LAF-1–RNA Interactions Are Correlated with LAF-1 Phase Boundary. To obtain molecular-level insight into the mechanism by which RNA interacts with and fluidizes LAF-1 droplets, we used single molecule FRET. We prepared a partially duplexed RNA, consisting of an 18-bp RNA duplex with a 50-nt polyU overhang. The FRET dye pair (Cy3 and Cy5) was situated at both extremities of the single-stranded RNA (ssRNA) to estimate the time-dependent distance changes between the two ends of the

ssRNA strand induced by LAF-1 binding (Fig. 4*A*). At 20 nM LAF-1 (above the K_D), we observe a high FRET peak, with a stable, nonfluctuating FRET signal indicative of static wrapping or compaction of RNA by LAF-1 (30) (dotted line at FRET values of ≈ 0.8; Fig. 4*B*). Interestingly, as the concentration of LAF-1 increases and approaches the phase boundary (≈ 0.8 µM), an additional broad FRET peak emerges, suggesting altered interactions between LAF-1 and the RNA substrate. The single molecule FRET traces reveal that the FRET changes arise from increased dynamics between LAF-1 and RNA, as evidenced by FRET fluctuations on increasing protein concentration. We note that the FRET fluctuations do not reflect successive binding and unbinding, as we do not observe fluctuations to the unbound RNA state ([Fig. S6](#)). We see a similar pattern when we use a fixed LAF-1 concentration, but approach the phase boundary by changing the salt concentration [NaCl] (Fig. 4*C*). Thus, interactions between LAF-1 and RNA become highly dynamic at protein and salt concentrations that favor droplet formation. This intermolecular dynamic behavior likely contributes to the fluidization of LAF-1 droplets by RNA (Fig. 3*A*).

The Disordered N-Terminal RGG Domain of LAF-1 Is Necessary and Sufficient for Phase Separation. We next sought to elucidate the molecular motifs that drive LAF-1 phase separation. Both the N and C termini of LAF-1 are predicted to be highly disordered, using the predictor of naturally disordered regions (PONDR) algorithm (31) (Fig. 5*A*). The N terminus of LAF-1 contains an arginine (R)/glycine (G)-rich domain with low sequence complexity, similar to the RGG domain known to bind RNA, whereas the shorter C terminus contains an R/G/Q-rich domain. We find that the C terminus is not required for phase separation, because LAF-1 with a deleted C terminus (∆C) still forms droplets in vitro (Fig. 5*C*), exhibiting a phase diagram similar to full-length (FL) LAF-1 ([Fig. S7](#)). In contrast, deletion of the RGG-rich N terminus (∆RGG) results in no observable droplets, even up to concentrations as high as 250 µM, revealing the N-terminal RGG domain as essential for phase separation. Moreover, the isolated N-terminal RGG domain was alone sufficient for forming droplets (Fig. 5*C*). To test the disorder prediction of this important domain, we performed circular dichroism (CD) measurements, which demonstrate a random coil signature (32) for the isolated RGG domain compared with the predominantly alpha-helical secondary structure of the FL and terminal deletions (Fig. 5*B*). Thus, the N-terminal RGG motif is intrinsically disordered and is responsible for driving LAF-1 phase separation into liquid-like droplets.
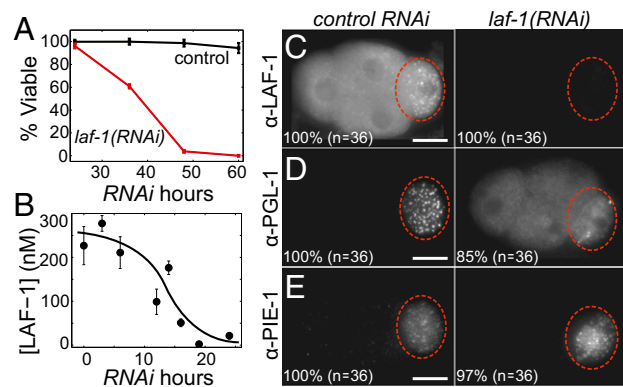

Fig. 6. LAF-1 depletion disrupts P granule organization. (*A*) The percentage of hatched embryos laid by singled hermaphrodites ($n = 42$) is strongly decreased in *laf-1(RNAi)* mothers. (*B*) Estimation of LAF-1 concentration in the germplasm as a function of *laf-1(RNAi)* exposure. (*C–E*) Epifluorescent images of four-cell embryos immunostained for LAF-1 (*C*), PGL-1 (*D*), and PIE-1 (*E*) at ≈ 30 h of RNAi feeding. (Scale bars, 10 µm.)
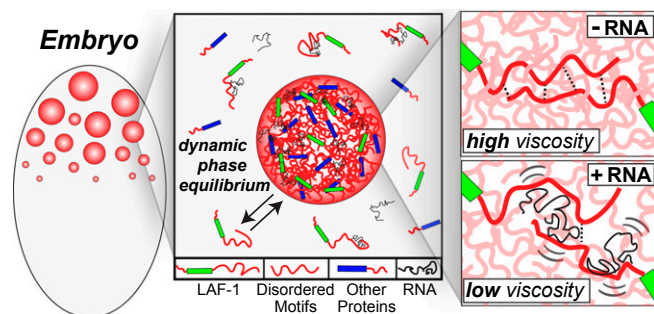
Fig. 7. Schematic illustrating the role of LAF-1 IDP motifs and RNA in droplet assembly and properties. IDP motifs (red) in LAF-1 (green) and likely other P granule proteins (blue) are important for driving phase separation into dynamic but coherent liquid droplets. These droplets are a liquid phase but with relatively high viscosity. RNA gives rise to dynamic interactions with LAF-1 (and likely other) IDP domains, modulating IDP–IDP interactions and leading to decreased droplet viscosity and increased molecular dynamics within the droplet.

Disordered domains often display dynamic binding behavior due to their conformational flexibility (33). Because the RGG domain is sufficient for RNA binding (Fig. S8), we asked whether the disordered RGG domain could be responsible for the observed dynamic binding to RNA. Applying our FRET assay to the truncation mutants, we find that both ΔC and the RGG domain alone exhibit highly dynamic FRET traces, similar to that seen in the full-length construct (Fig. 5D). However, ΔRGG gives rise to a static, tightly wrapped conformation of bound RNA, similar to that observed in non–droplet-forming conditions (Fig. 4 *B* and *C*). Thus, in addition to its role in driving phase separation, the disordered N-terminal RGG domain recapitulates the dynamic binding mode of the full-length protein.

RNAi Depletion of LAF-1 Disrupts P Granule Organization in the Early Embryo. Our finding that LAF-1 drives a liquid–liquid phase separation in vitro suggests that it may also drive assembly in vivo. Consistent with the embryonic lethality phenotype of *laf-1* mutants (20), we see a sharp decrease in the percentage of viable embryos on *laf-1(RNAi)* knockdown (Fig. 6A). Using mean fluorescence intensity analysis, we estimate the concentration of dilute LAF-1 in the untreated embryo cytoplasm to be ≈ 300 nM (*SI Text*), suggesting the total embryonic concentration is even higher. The concentration of embryonic LAF-1 drops by roughly 10-fold in the first 24 h of *laf-1(RNAi)* treatment (Fig. 6B). We observe that this strong decrease in LAF-1 concentration leads to a drastic decrease in PGL-1–positive granules in the progenitor germ cell, along with an increased cytoplasmic background concentration throughout the embryo (Fig. 6D). *laf-1(RNAi)* has no significant effect on the asymmetric segregation of PIE-1, indicating that polarity-dependent processes are not generally affected by loss of LAF-1 (Fig. 6E). The dissolution of PGL-1–positive granules on lowering of the LAF-1 concentration suggests that LAF-1 also promotes a liquid–liquid phase separation in vivo.

Discussion

An increasing body of work suggests that P granules and other RNP bodies assemble by a type of intracellular phase transition (2, 4, 7, 19). However, molecular-level insight into the components necessary to drive phase separation and maintain liquid-like properties is severely lacking. Here we showed that a single P granule protein, LAF-1, can drive phase separation in vitro, resulting in P granule-like liquid droplets. These data provide strong support for a role for LAF-1 in driving P granule assembly in vivo, by promoting cytoplasmic liquid–liquid phase separation. The contribution of LAF-1 to P granule assembly may be linked to the critical role played by LAF-1 in germ-line maintenance and

embryogenesis, underscored by the lethal and feminizing phenotype of LAF-1 mutants (20).

P granules are implicated in germ-line establishment and maintenance, but their precise function remains largely unknown. A recent study has shown that segregation of P granules to progenitor germ cells is only necessary for germ-line specification under certain conditions, suggesting a potential role for P granules in protection from stress (34); consistent with this, recent work has implicated LAF-1 and its close homolog VBH-1 in the stress response of *C. elegans* (35). P granules likely function in cytoplasmic RNA regulation, including storage and release of mRNA transcripts (36, 37). The liquid-like properties of P granules could facilitate their function as intracellular RNA microreactors, concentrating and colocalizing specific molecules, which nonetheless remain mobile within the droplet (25, 38). Our finding that LAF-1 droplet viscosity, and the dynamics of droplet components, can be tuned by both salt and RNA (Fig. 2) suggests the potential for functional feedback. In particular, the rate at which P granule components are stored, processed, and/or released should depend on viscosity and transport within P granules, which in turn can depend on the concentration of these same components. Such functional feedback could potentially be tuned throughout development, in parallel with altered germ-line RNA expression.

Our work demonstrates a key role for the N-terminal RGG domain of LAF-1. This region of LAF-1 is intrinsically disordered and is necessary and sufficient for phase separation (Fig. 4). Moreover, the RGG domain is also necessary and sufficient for the surprising RNA binding dynamics that coincide with the protein phase boundary. IDPs have remained largely mysterious and poorly understood, because they are outside of the traditional paradigm of stereospecific molecular interactions mediated by compact, well-folded 3D protein structure. However, it is estimated that as many as 30% (39) of proteins in the human genome have regions of intrinsic disorder, and IDPs appear to be involved in a range of biological functions, owing to their flexible conformations and binding promiscuity. Our findings are consistent with the emerging role of LCS/IDPs in promoting the assembly of RNP bodies (15, 16, 40–42).

The disordered N terminus is rich in arginines (R) and glycines (G) and is similar to the well-known RGG/RG motif RNA-binding domain (43). Several other P granule proteins, including PGL-1 and -3 and VBH-1 contain RGG-rich sequences similar to that of LAF-1, which are also predicted to be disordered. Intermolecular IDP interactions between LAF-1 and various P granule proteins could thus underlie maintenance of a dynamic but coherent P granule structure (Fig. 7). This picture is consistent with recent work suggesting a role in P granule assembly for two predicted IDP-containing proteins: MEG-1 and MEG-3 (41). The interactions between these proteins is controlled by phosphorylation, reflecting a balance between activity of the kinase MBK-2/DYRK and the phosphatase PPTR-1/2; this manifests in altered propensity for assembly of P granules. Such posttranslational modifications are likely to tune intermolecular interactions by regulating the charge state of IDPs (42), consistent with our findings on the salt and RNA dependence of LAF-1 droplet assembly and properties.

Our work shows that RNA does not shift the LAF-1 phase diagram (Fig. S4), despite contributing to a decrease in droplet viscosity. Thus the molecular interactions that give rise to the material properties within droplets are not necessarily equivalent to the interactions that govern droplet assembly. Droplet properties could also be affected by the predicted ATPase activity of the DEAD box helicase domain within LAF-1. Indeed, prior work on nucleoli suggests that the viscosity of RNP bodies may be ATP dependent (3). However, the experiments we performed here were done in the absence of ATP, and thus both assembly and RNA-mediated fluidization are independent of ATPase activity. Nonetheless, ATP could also play an important role in regulating P granule droplet properties and dynamics in vivo.

IDPs are closely related to LCS proteins, which have been suggested to promote RNP body formation by assembling into gel-like states (16, 17). However, our work here, performed using near-physiological buffer conditions, demonstrates that a P granule IDP assembles into purely viscous liquid droplets. These results are consistent with the idea that RNP assemblies lie on a viscoelastic spectrum, where solid-like states may be more typical of pathological extremes (19). The cell's ability to tune the properties of RNP bodies is likely to have important consequences for the biological function of these liquid phase organelles, underscored by the strong link we identified between droplet material properties and internal molecular dynamics. Elucidating the functional intracellular consequences of altered droplet properties remains an exciting and key future challenge.

Methods

Protein Purification. LAF-1 constructs with a C-terminal 6×-His tag were purified on Ni-NTA agarose resin (Qiagen) followed by a HiTrap Heparin column (GE) and flash frozen in high salt buffer (see *SI Text* for details).

Microrheology. Microrheology was performed as previously described (5). PEGylated fluorescent microspheres were added to low salt buffer before being mixed with a small volume of concentrated protein in high salt solution. Bead diffusion was tracked on a spinning disk confocal microscope for 500 s using 500-ms intervals. MSD data were fit (Fig. S2A) to the form $MSD(\tau) = 4D\tau^{\alpha} + NF$ where α is the diffusive exponent, D is the diffusion coefficient, and NF is a constant representing the noise floor (see *SI Text* for details).

See *SI Text* for FRAP, single molecule FRET, and CD spectroscopy methods in detail.

1. Anderson P, Kedersha N (2006) RNA granules. *J Cell Biol* 172(6):803–808.
2. Brangwynne CP, et al. (2009) Germline P granules are liquid droplets that localize by controlled dissolution/condensation. *Science* 324(5935):1729–1732.
3. Brangwynne CP, Mitchison TJ, Hyman AA (2011) Active liquid-like behavior of nucleoli determines their size and shape in Xenopus laevis oocytes. *Proc Natl Acad Sci USA* 108(11):4334–4339.
4. Wippich F, et al. (2013) Dual specificity kinase DYRK3 couples stress granule condensation/dissolution to mTORC1 signaling. *Cell* 152(4):791–805.
5. Feric M, Brangwynne CP (2013) A nuclear F-actin scaffold stabilizes RNP droplets against gravity in large cells. *Nat Cell Biol* 15(10):1253–1259.
6. Hubstenberger A, Noble SL, Cameron C, Evans TC (2013) Translation repressors, an RNA helicase, and developmental cues control RNP phase transitions during early development. *Dev Cell* 27(2):161–173.
7. Weber SC, Brangwynne CP (2015) Inverse size scaling of the nucleolus by a concentration-dependent phase transition. *Curr Biol* 25(5):641–646.
8. Li P, et al. (2012) Phase transitions in the assembly of multivalent signalling proteins. *Nature* 483(7389):336–340.
9. Voronina E, Seydoux G, Sassone-Corsi P, Nagamori I (2011) RNA granules in germ cells. *Cold Spring Harb Perspect Biol* 3(12):3.
10. Lee CF, Brangwynne CP, Gharakhani J, Hyman AA, Jülicher F (2013) Spatial organization of the cell cytoplasm by position-dependent phase separation. *Phys Rev Lett* 111(8):088101.
11. Updike D, Strome S (2010) P granule assembly and function in Caenorhabditis elegans germ cells. *J Androl* 31(1):53–60.
12. Yarunin A, Harris RE, Ashe MP, Ashe HL (2011) Patterning of the Drosophila oocyte by a sequential translation repression program involving the d4EHP and Belle translational repressors. *RNA Biol* 8(5):904–912.
13. Beckham C, et al. (2008) The DEAD-box RNA helicase Ded1p affects and accumulates in Saccharomyces cerevisiae P-bodies. *Mol Biol Cell* 19(3):984–993.
14. Shih JW, et al. (2012) Critical roles of RNA helicase DDX3 and its interactions with eIF4E/PABP1 in stress granule assembly and stress response. *Biochem J* 441(1):119–129.
15. Uversky VN, Kuznetsova IM, Turoverov KK, Zaslavsky B (2015) Intrinsically disordered proteins as crucial constituents of cellular aqueous two phase systems and coacervates. *FEBS Lett* 589(1):15–22.
16. Kato M, et al. (2012) Cell-free formation of RNA granules: Low complexity sequence domains form dynamic fibers within hydrogels. *Cell* 149(4):753–767.
17. Han TW, et al. (2012) Cell-free formation of RNA granules: Bound RNAs identify features and components of cellular assemblies. *Cell* 149(4):768–779.
18. Decker CJ, Teixeira D, Parker R (2007) Edc3p and a glutamine/asparagine-rich domain of Lsm4p function in processing body assembly in Saccharomyces cerevisiae. *J Cell Biol* 179(3):437–449.
19. Weber SC, Brangwynne CP (2012) Getting RNA and protein in phase. *Cell* 149(6):1188–1191.
20. Goodwin EB, Hofstra K, Hurney CA, Mango S, Kimble J (1997) A genetic pathway for regulation of tra-2 translation. *Development* 124(3):749–758.
21. Hubert A, Anderson P (2009) The C. elegans sex determination gene laf-1 encodes a putative DEAD-box RNA helicase. *Dev Biol* 330(2):358–367.

22. Asherie N (2004) Protein crystallization and phase diagrams. *Methods* 34(3):266–272.
23. Dill KA, Bromberg S (2011) *Molecular Driving Forces: Statistical Thermodynamics in Biology, Chemistry, Physics, and Nanoscience* (Garland Science, New York).
24. Debenedetti PG (1996) *Metastable Liquids: Concepts and Principles* (Princeton Univ Press, Princeton).
25. Brangwynne CP (2011) Soft active aggregates: Mechanics, dynamics and self-assembly of liquid-like intracellular protein bodies. *Soft Matter* 7(7):3052–3059.
26. Mason TG, Weitz DA (1995) Optical measurements of frequency-dependent linear viscoelastic moduli of complex fluids. *Phys Rev Lett* 74(7):1250–1253.
27. Larson RG (1999) *The Structure and Rheology of Complex Fluids* (Oxford Univ Press, New York).
28. Howard J (2001) *Mechanics of Motor Proteins and the Cytoskeleton* (Sinauer Associates, Sunderland, MA).
29. Aarts DG, Schmidt M, Lekkerkerker HN (2004) Direct visual observation of thermal capillary waves. *Science* 304(5672):847–850.
30. Roy R, Kozlov AG, Lohman TM, Ha T (2007) Dynamic structural rearrangements between DNA binding modes of E. coli SSB protein. *J Mol Biol* 369(5):1244–1257.
31. Xue B, Dunbrack RL, Williams RW, Dunker AK, Uversky VN (2010) PONDR-FIT: A metapredictor of intrinsically disordered amino acids. *Biochim Biophys Acta* 1804(4):996–1010.
32. Chen YH, Yang JT, Martinez HM (1972) Determination of the secondary structures of proteins by circular dichroism and optical rotatory dispersion. *Biochemistry* 11(22):4120–4131.
33. Dyson HJ, Wright PE (2005) Intrinsically unstructured proteins and their functions. *Nat Rev Mol Cell Biol* 6(3):197–208.
34. Gallo CM, Wang JT, Motegi F, Seydoux G (2010) Cytoplasmic partitioning of P granule components is not required to specify the germline in C. elegans. *Science* 330(6011):1685–1689.
35. Paz-Gómez D, Villanueva-Chimal E, Navarro RE (2014) The DEAD Box RNA helicase VBH-1 is a new player in the stress response in C. elegans. *PLoS ONE* 9(5):e97924.
36. Sheth U, Pitt J, Dennis S, Priess JR (2010) Perinuclear P granules are the principal sites of mRNA export in adult C. elegans germ cells. *Development* 137(8):1305–1314.
37. Voronina E (2013) The diverse functions of germline P-granules in Caenorhabditis elegans. *Mol Reprod Dev* 80(8):624–631.
38. Hyman AA, Brangwynne CP (2011) Beyond stereospecificity: Liquids and mesoscale organization of cytoplasm. *Dev Cell* 21(1):14–16.
39. Ward JJ, Sodhi JS, McGuffin LJ, Buxton BF, Jones DT (2004) Prediction and functional analysis of native disorder in proteins from the three kingdoms of life. *J Mol Biol* 337(3):635–645.
40. Toretsky JA, Wright PE (2014) Assemblages: Functional units formed by cellular phase separation. *J Cell Biol* 206(5):579–588.
41. Wang JT, et al. (2014) Regulation of RNA granule dynamics by phosphorylation of serine-rich, intrinsically disordered proteins in C. elegans. *eLife* 3:e04591.
42. Nott TJ, et al. (2015) Phase transition of a disordered nuage protein generates environmentally responsive membraneless organelles. *Mol Cell* 57(5):936–947.
43. Thandapani P, O'Connor TR, Bailey TL, Richard S (2013) Defining the RGG/RG motif. *Mol Cell* 50(5):613–623.